JOURNAL OF COMPUTATIONAL PHYSICS 91, 398–412 (1990)

On Far-Field Stream Function Condition for Two-Dimensional Incompressible Flows

JONG-YOUB SA* AND KEUN-SHIK CHANG

Department of Mechanical Engineering, KAIST, P.O. Box 150, Cheongryang, Seoul, Republic of Korea

Received August 1, 1988; revised September 13, 1989

An expression for the stream function at a far field boundary is derived from the Poisson integral in a series form of inverse powers of the radial distance r. The present formulation allows solid body or bodies to be contained within an open domain, contrary to the earlier ones. Accuracy of this far boundary condition has been tested on three model flows (starting, steady, and periodic flows) with computational domains of which outer-boundary radius widely varies. The present boundary condition is excellent, especially for the starting flow. For the periodic flow, the present boundary condition still performed best in comparison with conventional far boundary conditions while the Neumann condition, which had comparable accuracy with less computation time for the steady flow, failed altogether to achieve any convergence.

1. INTRODUCTION

For a concentrated vortical flow dominated by diffusion in an open domain, it is well known that the vorticity spatially decays faster than the velocity. However, the vorticity-stream function formulation requires some caution at a far field computational boundary because of the slow spatial convergence of the stream function to the free stream values. A variety of techniques have been used in the literature for the far-field stream function condition [1–12]: the free stream values, the potential flow, and the Neumann condition for the perturbed stream function. The computational domain in these methods, however, should be as large as possible to reduce the error caused by the inaccurate description of the far boundary condition.

Chamberlain and Liu [13] used a series form of the vector potential developed by Ting [14] to compute the interaction of two mutually interacting vortex rings, but the method does not allow solid bodies to be present within the computational domain. This method has been extended by the present authors [15] to a viscous vortex ring reflected from an infinite flat wall. The present far-field stream function condition of integral series form is developed to allow general solid body or bodies to be contained within the domain. The accuracy of the method has been tested on three model problems: the starting flow, the steady-state flow, and the periodic flow

* Present address is NASA Ames Research Center, MS 258-1, Moffett Field, CA 94035.

0021-9991/90 $3.00

past a circular cylinder. Computational domains of which the outer-boundary radius widely varies are considered and comparison of results among different methods is made.

2. The Governing Equations

We consider two-dimensional incompressible viscous flow past a circular cylinder of radius a in an unbounded domain shown in Fig. 1. Here, U_0 is the free stream velocity and r_∞ is the radius of computational domain.

The vorticity and stream function equations are first written in the cylindrical polar coordinate system. For the purpose of coordinate stretching toward the cylinder we use the transformation $r = e^{\pi\xi}$ and $\theta = \pi\eta$, by which the governing equations take the following conservation form

$$\frac{\partial \zeta}{\partial t} + \frac{1}{(\pi r)^2}\left(\frac{\partial}{\partial \xi}\left(\zeta \frac{\partial \psi}{\partial \eta}\right) - \frac{\partial}{\partial \eta}\left(\zeta \frac{\partial \psi}{\partial \xi}\right)\right) = \frac{2}{Re}\tilde{\nabla}^2 \zeta \tag{1}$$

$$\tilde{\nabla}^2 \psi = -\zeta \tag{2}$$

where

$$\tilde{\nabla}^2 \equiv \frac{1}{(\pi r)^2}\left(\frac{\partial^2}{\partial \xi^2} + \frac{\partial^2}{\partial \eta^2}\right)$$

$$Re = \frac{(2a)\, U_0}{\nu}.$$

The contravariant velocity components in the convection term, the derivatives $\partial\psi/\partial\xi$ and $\partial\psi/\partial\eta$, are computed by the fourth-order Hermitian relation given below [16]. This special numerical treatment will allow the finite difference method to

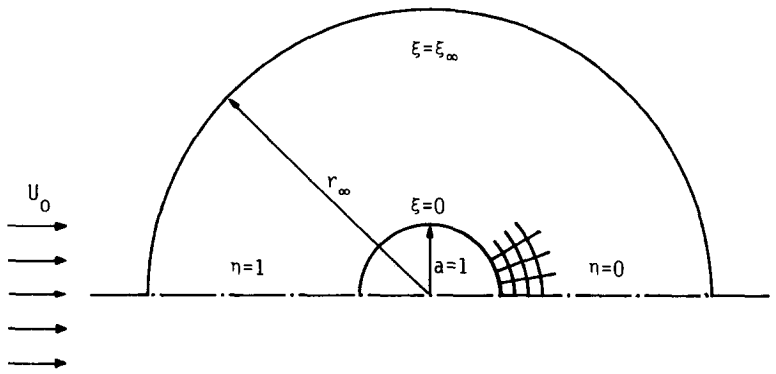

FIG. 1. The problem configuration.

retain second-order spacewise accuracy endowed by the central differencing of other spatial derivatives,

$$\psi_{\xi_{i-1,j}} + 4\psi_{\xi_{i,j}} + \psi_{\xi_{i+1,j}} = \frac{3}{\Delta\xi}(\psi_{i+1,j} - \psi_{i-1,j}) + O(\Delta\xi^4) \tag{3}$$

$$\psi_{\eta_{i,j-1}} + 4\psi_{\eta_{i,j}} + \psi_{\eta_{i,j+1}} = \frac{3}{\Delta\eta}(\psi_{i,j+1} - \psi_{i,j-1}) + O(\Delta\eta^4). \tag{4}$$

The appropriate boundary conditions for the vorticity and stream function would be

$$\begin{aligned}
&\text{at } \xi = 0 \qquad \zeta_w = -\psi_\xi|_{w+1}/((\pi r)^2\,\Delta\xi)\\
&\qquad\qquad \psi_w = 0\\
&\text{at } \xi = \xi_\infty \qquad \zeta_\infty = 0 \qquad \left(\text{at in-flow boundary where } \frac{\partial\psi}{\partial\eta} < 0\right)\\
&\qquad\qquad \left.\frac{\partial\zeta}{\partial\xi}\right|_\infty = 0 \qquad \left(\text{at out-flow boundary where } \frac{\partial\psi}{\partial\eta} > 0\right)\\
&\qquad\qquad \psi_\infty = \psi_{\text{far}} \qquad \text{(at entire far boundary).}
\end{aligned}$$

A homogeneous boundary condition is applied for both ζ and ψ on the line of symmetry, $\eta = 0$ and 1, in the case of starting and steady-state flow. For the flow, which is not symmetric, i.e., on exhibiting periodic vortex shedding, the condition of spartial periodicity must be applied on $\eta = 0$ and 2.

The far boundary stream function, ψ_∞, can be treated in a variety of ways. If the free stream is superposed by a perturbation as

$$\psi = \psi^0 + \psi' \qquad (\psi^0 = U_0\, y) \tag{5}$$

then the perturbed stream function at infinity may be treated in four different ways as

(1) the integral-series expansion

$$\psi'_\infty = \frac{1}{2\pi}\sum_{n=1}^{5}\frac{1}{n}G_n \sin(n\theta)\, r_\infty^{-n} \tag{6}$$

(2) the free stream condition

$$\psi'_\infty = 0 \tag{7}$$

(3) the potential flow condition

$$\psi'_\infty = -\sin\theta r_\infty^{-1} \tag{8}$$

(4) the Neumann condition

$$\frac{\partial \psi'_\infty}{\partial \xi} = 0. \tag{9}$$

The boundary condition (6), when superimposed with the base flow, ψ^0, constitutes the far-boundary stream function ψ_∞ used in the present method.

The vorticity transport equation (1) is solved for the unsteady case by the Euler explicit method and for the steady case by the Euler implicit method for fast convergence. To save computing time for the time-marching cases, the Poisson equation (2) is numerically integrated by a direct elliptic solver called the SEVP (stabilized error vector propagating) method, devised by Madala [17]. For the steady flows, however, an iterative method such as the point SOR would be equally good to get the equilibrium solution of the Poisson equation.

3. Integral-Series Method

Consider the Poisson equation of the stream function

$$\nabla^2 \psi = -\zeta \tag{10}$$

The following integral equation can be easily derived for the flow with free-stream velocity (U_0, V_0) on an open domain

$$\psi(\mathbf{r}) = U_0 y - V_0 x - \frac{1}{2\pi}\left\{\iint_\Omega \zeta(\mathbf{r}) \ln(|\mathbf{r}_0 - \mathbf{r}|)\, dS(\mathbf{r}_0) + \int_{\Gamma_w} V_b(\mathbf{r}_0) \ln(|\mathbf{r}_0 - \mathbf{r}|)\, dl(\mathbf{r}_0)\right\}, \tag{11}$$

where $\mathbf{r}_0$ is the integration variable and V_b is the tangential velocity defined positive in the counterclockwise direction on the body. The two integrals in Eq. (11) can be expressed on a far boundary by an inverse power series of r, as demonstrated in the Appendix. Eq. (11) then becomes

$$\psi_\infty(r, \theta) = U_0 y - V_0 x - \frac{(F_0 + A_0)}{2\pi} \ln(r) + \frac{1}{2\pi} \sum_{n=1}^{5} \frac{1}{n} \{(F_n + A_n) \cos(n\theta) + (G_n + B_n) \sin(n\theta)\}\, r^{-n} + O(r^{-6}). \tag{12}$$

If the circular cylinder is stationary relative to the flow, the coefficients A_n and B_n vanish. If the flow is symmetric, F_n also becomes zero. Equation (12) then simply becomes

$$\psi = U_0 y + \frac{1}{2\pi} \sum_{n=1}^{5} \frac{1}{n} G_n \sin(n\theta)\, r^{-n} + O(r^{-6}), \tag{13}$$

where

$$G_1 = 2 \iint \zeta y \, dS,$$

$$G_2 = 2 \iint 2\zeta xy \, dS,$$

$$G_3 = 2 \iint \zeta(3x^2 y - y^3) \, dS,$$

$$G_4 = 2 \iint \zeta(4x^3 y - 4xy^3) \, dS,$$

$$G_5 = 2 \iint \zeta(5x^4 y - 10x^2 y^3 + y^5) \, dS.$$

Here the vorticity in the above integrations is calculated from Eq. (1). In the case when the flow is asymmetric, the full (not symmetric half) domain should be considered for integration. The factor 2 in front of the integrals should then also dropped from the G_n expressions. When there are vortices alternately shed from the cylinder, the neighboring vortices have opposite signs which fortunately lead to the inequality $F_n \ll G_n$. The right-hand side of Eq. (13) consists of the free stream value (the first term) and the correction terms in series form made of G_n contribution which have been neglected altogether in the conventional formulations. This integral series, expanded up to five terms in the present formulation, plays a significant role in the practical computation, since the computational domain cannot be taken as infinite. The integrals in the above coefficients consume some computer time; however, the vorticity is nearly zero at most grid points. That is, the vorticity generated on the surface of the body is transported to a limited region by means of convection and diffusion. In the unsteady problem, computer time increased due to the above G_n integrals was merely about 10% per time step when the direct elliptic solver was adopted for the stream-function Poisson equation. The computer cost would become relatively even less if an iterative method were employed for the unsteady problem.

4. Result and Discussion

In the first two test computations at $Re = 20$ (the impulsive starting of the circular cylinder with the potential flow as an initial condition and the steady-state vortical flow), the upper half domain only was considered ($0 \leqslant \xi \leqslant \xi_\infty$, $0 \leqslant \eta \leqslant 1$).

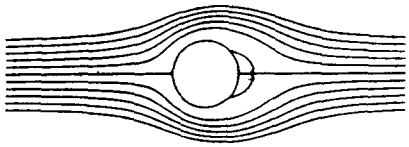

(a) starting flow (Re=20, t=2)

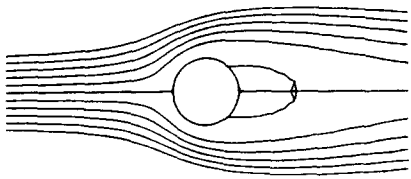

(b) steady flow (Re=20)

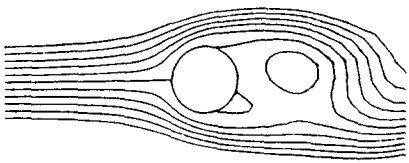

(c) periodic flow (Re=100)

FIG. 2. Three model flow problems.

In these two test computations of the present paper, constant step size were used as $\Delta\eta = \frac{1}{30}$, $\Delta\xi = 0.02$, and $\Delta t = 0.01$. In Fig. 2 the three model fluid flows computed in the present study (the last is a strictly periodic flow requiring a full computational domain) are represented by the instantaneous streamline plots: the integral-series boundary condition is used for all the cases at $r_\infty = 23.1$.

The four different far-boundary conditions yield essentially the same flow field when sufficiently large computational domain is employed. We computed the flow for a circular cylinder under impulsive starting ($r \leqslant 6.6$), with the far-boundary condition at the radius $r_\infty = 81.3$ ($\xi_\infty = 70\,\Delta\xi$) as shown in Fig. 3. The perturbed stream function ψ' and the vorticity ζ were observed to have virtually identical contours among the various boundary conditions in this large computational domain. We will refer to this flow computed with $r_\infty = 81.3$ as the "standard solution."

As the computational domain is progressively reduced, there is a deviation of the various numerical results from this standard solution. Figure 4 represents the functional contours obtained for $r_\infty = 23.1$ ($\xi_\infty = 50\,\Delta\xi$), and Fig. 5 for even smaller computational domains. The vorticity contours are well coincident for the different boundary conditions, a result that is expected from the behavior of vorticity decaying exponentially. The perturbed stream function, however, decays very slowly as seen from the inverse series of r in Eq. (13); its consequence is well represented in Fig. 4

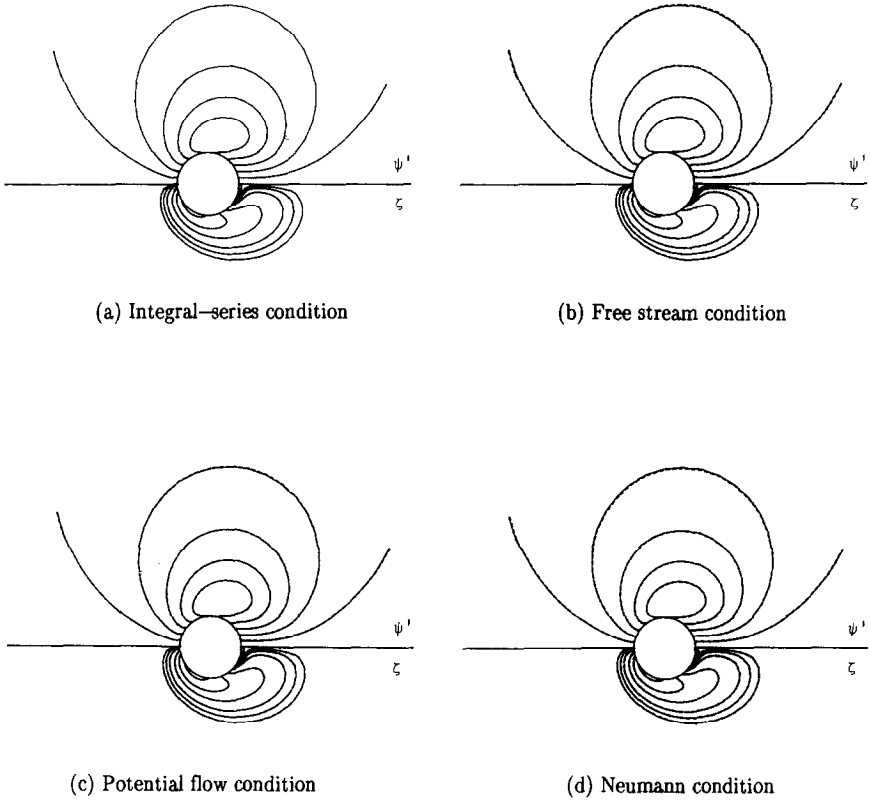

(a) Integral–series condition (b) Free stream condition

(c) Potential flow condition (d) Neumann condition

FIG. 3. Four boundary conditions with $r_\infty = 81.3$ show identical result in the area $r \leqslant 6.6$, at $Re = 20$ and $t = 2$; the dotted lines in (b), (c), and (d) are the result from the integral-series condition.

by the deviation from the standard solution for methods other than integral series. The integral series condition retains accuracy as the computational domain is even further reduced: the computational domain in Fig. 5 is as small as $r_\infty = 6.6$ ($\xi_\infty = 30\,\Delta\xi$) and $r_\infty = 3.5$ ($\xi_\infty = 20\,\Delta\xi$). These results suggest that as long as the vorticity remains confined and concentrated inside the computational domain, the use of the integral series boundary condition gives accurate solutions, even with a very limited computational domain.

Figure 6 represents the time history of the drag coefficients C_D with $r_\infty = 6.6$ for the starting cylinder problem up to the time (scaled by a/U_0) $t = 2$. The integral series condition perfectly follows the standard solution while the other far-boundary conditions offer either over- or under-prediction. Figure 7 shows the drag coefficient at an instant $t = 2$ computed with various sizes of computational domain. The severe domain-dependency of the computed results for the methods other than the integral series is evident.

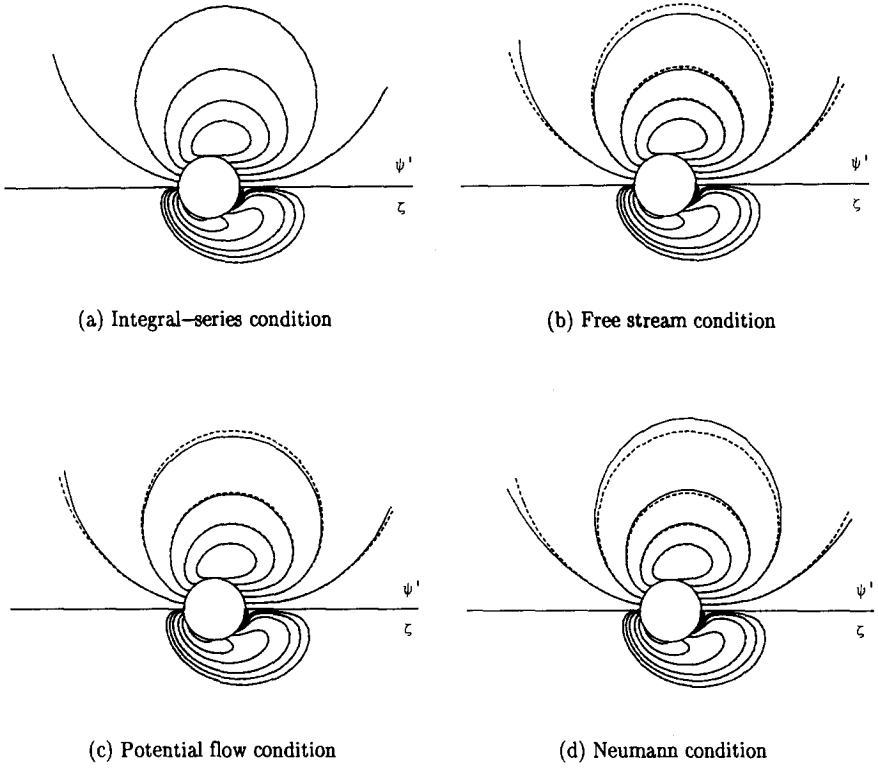

(a) Integral–series condition (b) Free stream condition

(c) Potential flow condition (d) Neumann condition

FIG. 4. The stream function and vorticity contours with $r_\infty = 23.1$ ($Re = 20$, $t = 2$). The dotted lines represent the standard solution.

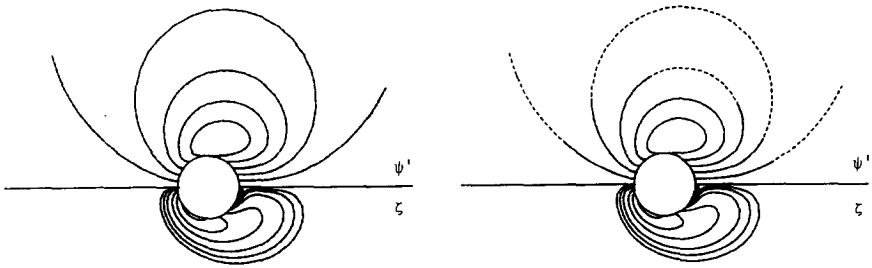

(a) r_∞=6.6 (Integral–series condition) (b) r_∞=3.5 (Integral–series condition)

FIG. 5. The stream function and vorticity contours with further reduced domain. The dotted lines represent the standard solution.

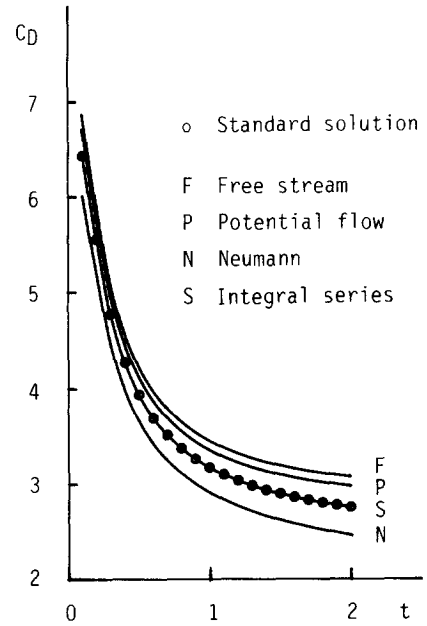

FIG. 6. The time history of drag coefficient with $r_\infty = 6.6$ for the starting flow, $Re = 20$.

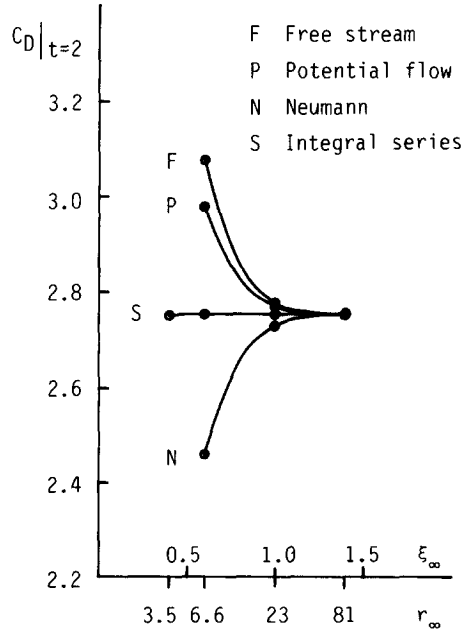

FIG. 7. Domain-dependency of the computation for the starting flow at $Re = 20$, $t = 2$.

The steady-state flow past a circular cylinder has twin vortex attached to the body at $Re = 20$, and the vorticity in the wake leaves the computational domain across the outflow boundary. It makes the numerical solutions more domain-dependent as shown in Fig. 8 (the numerical data is given in Table I). The present boundary condition shows still better accuracy when compared with others. Nevertheless, for the steady-state flow using the point-SOR method, the Neumann condition turned out to have the best performance because of large computation time of the integral series method (about 100% increase per each iteration).

The computed results for a strictly periodic flow at $Re = 100$ having alternating vortex shedding is represented in Fig. 9. The mean drag coefficient and the Strouhal number of the vortex shedding, $St = f(2a)/U_0$, are plotted separately. The computational domain is full in this case with $0 \leqslant \xi \leqslant \xi_\infty$ and $0 \leqslant \eta \leqslant 2$ ($\Delta\xi = 0.02$, $\Delta\eta = \frac{2}{50}$, $\Delta t = 0.05$). The Neumann condition failed to yield any converged solution even with the largest domain tried, $r_\infty = 81.3$. The present integral series method showed the least sensitivity to the size of the computational domain, and its result stayed nearest to the asymptotic value obtainable with the large computational radius $r_\infty = 81.3$. For the range of computational domain tested, $12.3 \leqslant r_\infty \leqslant 43.4$, the numerical result of the mean drag coefficient by the integral series method had a 2.2% variation while the other boundary conditions showed variation up to 8.2%.

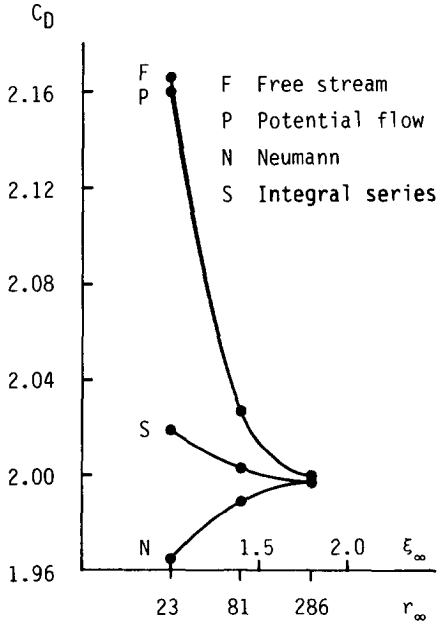

FIG. 8. Domain-dependency of the computation for the steady flow at $Re = 20$.

TABLE I

Comparison of the Drag Coefficient for the Steady Flow at $Re = 20$

Boundary conditions	$r_\infty = 23$	81	286
Free stream	2.166	2.028	2.001
Potential flow	2.160	2.028	2.001
Integral series	2.020	2.004	1.997
Neumann	1.965	1.989	1.997

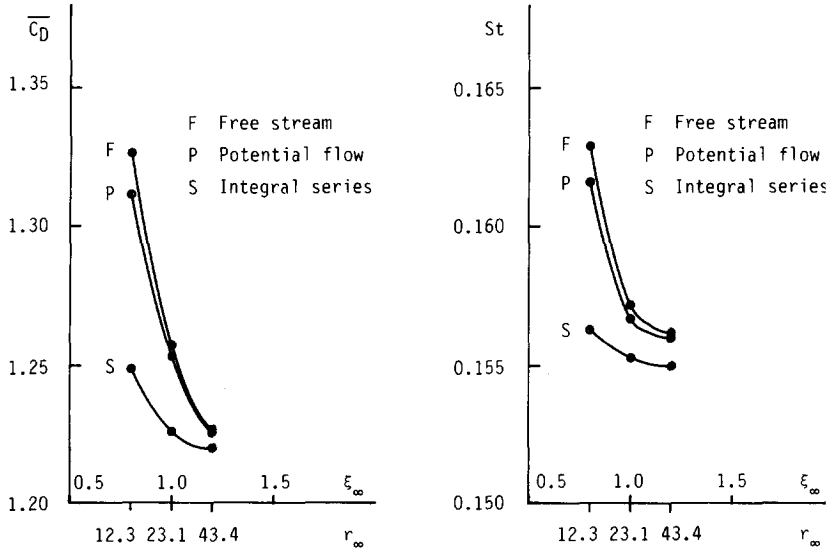

(a) Drag coefficient

(b) Strouhal number

FIG. 9. Domain-dependency of the computation for the periodic flow at $Re = 100$.

5. Conclusion

The integral series expansion of the stream function has been demonstrated to be useful as a far-field computational boundary condition. For the unsteady problems using a direct elliptic solver, the implementation requires only a modest amount of extra work (about 10% per time step) over other boundary conditions which have been used. The present study indicated that the use of integral-series boundary condition was excellent, especially for the starting flow. As long as the vorticity was contained within the computational domain, the method was accurate enough to yield virtually identical results for two widely different domains, $r_\infty = 3.5$ and $r_\infty = 81.3$. In the case when the vorticity left the domain across the outflow boundary, accuracy was degraded because the vorticity did not decay fast in the wake region. Nevertheless, the present study also indicated that the use of the integral-series condition still gave the best results for the periodic flow; for the steady flow, however, the Neumann condition gave comparable accuracy with less computation time despite its incapability of treating periodic flow with vortex shedding. The present method is applicable to the general two-dimensional problems having arbitrary body or bodies inside an open domain.

Appendix

From Eq. (11),

$$\psi(\mathbf{r}) = Uy - Vx - \frac{1}{2\pi}\iint_{\Omega} \zeta_0 \ln(r')\, dS_0 - \frac{1}{2\pi}\int_{\Gamma_w} V_{b_0} \ln(r')\, dl_0. \tag{A.1}$$

Consider the function in the (r, θ) coordinate system

$$\phi(r, \theta) = \frac{1}{2\pi}\iint \zeta_0 \ln(r')\, dS_0. \tag{A.2}$$

If we identify points in the plane with complex values and let $z = re^{i\theta}$, then we can write the function ϕ as

$$\begin{aligned}
\phi(z) &= \frac{1}{2\pi}\,\Re\left[\iint \ln(z - z_0)\,\zeta_0\, dS_0\right] \\
&= \frac{1}{2\pi}\,\Re\left[\iint \ln\left(z\left(1 - \frac{z_0}{z}\right)\right)\zeta_0\, dS_0\right] \\
&= \frac{1}{2\pi}\,\Re\left[\iint \ln(z)\,\zeta_0\, dS_0 + \iint \ln\left(1 - \frac{z_0}{z}\right)\zeta_0\, dS_0\right].
\end{aligned} \tag{A.3}$$

Here $\Re$ is the real part of the expression. The first integral in the above expression becomes merely

$$\frac{1}{2\pi}\iint \ln(r)\,\zeta_0\,dS_0$$

while in the second integral we can use the expansion

$$\ln\left(1-\frac{z_0}{z}\right)=-\sum_{k=1}^{\infty}\frac{1}{k}\left(\frac{z_0}{z}\right)^k,$$

since our test point z is outside a circle containing z_0. Substituting this expression in the integral and interchanging integration and summation, yield

$$\frac{1}{2\pi}\Re\left[\iint \ln\left(1-\frac{z_0}{z}\right)\zeta_0\,dS_0\right]=-\sum_{k=1}^{\infty}\frac{1}{2\pi}\Re\left[\iint\frac{1}{k}\left(\frac{z_0}{z}\right)^k\zeta_0\,dS_0\right].$$

Now

$$\Re\left[\left(\frac{z_0}{z}\right)\right]=r^{-k}((r_0^k\cos(k\theta_0))\cos(k\theta)+(r_0^k\sin(k\theta_0))\sin(k\theta)).$$

So

$$\begin{aligned}\phi(r,\theta)=&\frac{1}{2\pi}\iint\ln(r)\,\zeta_0\,dS_0\\&-\sum_{k=1}^{\infty}\left(\frac{1}{2\pi k}\iint r_0^k\cos(k\theta_0)\,\zeta_0\,dS_0\right)r^{-k}\cos(k\theta)\\&+\left(\frac{1}{2\pi k}\iint r_0^k\sin(k\theta_0)\,\zeta_0\,dS_0\right)r^{-k}\sin(k\theta).\end{aligned}\tag{A.4}$$

One can express the integrals in the above expansion in terms of the variables (x, y) by noting that

$$\begin{aligned}r_0^k\cos(k\theta_0)&=\Re[(r_0\cos(\theta_0)+ir_0\sin(\theta_0))^k]\\&=\Re[(x_0+iy_0)^k].\end{aligned}$$

The imaginary part of $(x_0+iy_0)^k$ is used to express $r_0^k\sin(k\theta_0)$ as a polynomial in x_0 and y_0. When written in terms of (x, y), the function $\phi(r, \theta)$ now becomes

$$\phi(r,\theta)=\frac{1}{2\pi}\langle\zeta_0\rangle\ln(r)$$
$$-\{\langle\zeta_0 x_0\rangle\cos\theta+\langle 2\zeta_0 x_0 y_0\rangle\sin\theta\}$$
$$-\{\langle\zeta_0(x_0^2-y_0^2)\rangle\cos 2\theta+\langle 2\zeta_0 x_0 y_0\rangle\sin 2\theta\}$$
$$-\{\langle\zeta_0(x_0^3-3x_0 y_0^2)\rangle\cos 3\theta+\langle\zeta_0(3x_0^2 y_0-y_0^3)\rangle\sin 3\theta\}$$
$$-\{\langle\zeta_0(x_0^4-6x_0^2 y_0^2+y_0^4)\rangle\cos 4\theta+\langle\zeta(4x_0^3 y_0-4x_0 y_0^3)\rangle\sin 4\theta\}$$
$$-\{\langle\zeta_0(x_0^5-10x_0^3 y_0^2+5x_0 y_0^4)\rangle\cos 5\theta$$
$$+\langle\zeta_0(5x_0^4 y_0-10x_0^2 y_0^3+y_0^5)\rangle\sin 5\theta\}, \tag{A.5}$$

where $\langle\ \rangle\equiv\iint_\Omega dS_0$.

The last term of Eq. (A.1) follows a similar process and Eq. (A.1) finally takes the form

$$\psi_{\text{far}}=Uy-Vx-\frac{(F_0+A_0)}{2\pi}\ln(r)$$
$$+\frac{1}{2\pi}\sum_{n=1}^{5}\frac{1}{n}\{(F_n+A_n)\cos(n\theta)+(G_n+B_n)\sin(n\theta)\}\,r^{-n}+O(r^{-6}), \tag{A.6}$$

where

$$F_0=\iint\zeta\,dS,$$

$$F_1=\iint\zeta x\,dS, \qquad G_1=\iint\zeta y\,dS,$$

$$F_2=\iint\zeta(x^2-y^2)\,dS, \qquad G_2=\iint 2\zeta xy\,dS,$$

$$F_3=\iint\zeta(x^3-3xy^2)\,dS, \qquad G_3=\iint\zeta(3x^2y-y^3)\,dS,$$

$$F_4=\iint\zeta(x^4-6x^2y^2+y^4)\,dS, \qquad G_4=\iint\zeta(4x^3y-4xy^3)\,dS,$$

$$F_5=\iint\zeta(x^5-10x^3y^2+5xy^4)\,dS, \qquad G_5=\iint\zeta(5x^4y-10x^2y^3+y^5)\,dS,$$

$$A_0=\int V_b\,dl,$$

$$A_1=\int V_b x\,dl, \qquad B_1=\int V_b y\,dl,$$

$$A_2 = \int V_b(x^2 - y^2)\, dl, \qquad B_2 = \int 2V_b xy\, dl,$$

$$A_3 = \int V_b(x^3 - 3xy^2)\, dl, \qquad B_3 = \int V_b(3x^2y - y^3)\, dl,$$

$$A_4 = \int V_b(x^4 - 6x^2y^2 + y^4)\, dl, \qquad B_4 = \int V_b(4x^3y - 4xy^3)\, dl,$$

$$A_5 = \int V_b(x^5 - 10x^3y^2 + 5xy^4)\, dl, \qquad B_5 = \int V_b(5x^4y - 10x^2y^3 + y^5)\, dl.$$

REFERENCES

1. A. RINALDO AND A. GIORGINI, *Int. J. Numer. Methods* **4**, 949 (1984).
2. T. P. LOC AND R. BOUARD, *J. Fluid Mech.* **160**, 93 (1985).
3. W. M. COLLINS AND S. C. R. DENNIS, *J. Fluid Mech.* **60**, 105 (1973).
4. J. S. SON AND T. J. HANRATTY, *J. Fluid Mech.* **35**, 369 (1969).
5. H. JAFROUDI AND H. T. YANG, *J. Comput. Phys.* **49**, 181 (1983).
6. S. C. R. DENNIS AND G.-Z. CHANG, *J. Fluid Mech.* **42**, 471 (1970).
7. A. E. HAMIELEC AND J. D. RAAL, *Phys. Fluids* **12**, 11 (1969).
8. H. TAKAMI AND H. B. KELLER, *Phys. Fluids* **SII**, 51 (1969).
9. R. L. UNDERWOOD, *J. Fluid Mech.* **37**, 95 (1969).
10. S. K. JORDAN AND J. E. FROMM, *Phys. Fluids* **15**, 371 (1972).
11. Y. LECOINTE AND J. PIQUET, *Comput. Fluids* **12**, 255 (1984).
12. A. BORTHWICK, *Int. J. Numer. Methods* **6**, 275 (1986).
13. J. P. CHAMBERLAIN AND C. H. LIU, "Navier–Stokes Calculations for Unsteady Three-Dimensional Vortical Flows in Unbounded Domains," AIAA 84-0418, AIAA 22nd Aerospace Science Meeting, Reno, Nevada, Jan. 9, 1984.
14. L. TING, *J. Fluid Mech.* **127**, 497 (1983).
15. J. Y. SA, K. S. CHANG, AND C. H. LIU, "Wall Reflection of a Viscous Vortex Ring," AIAA 86-0561, AIAA 24th Aerospace Science Meeting, Reno, Nevada, Jan. 6, 1986.
16. T. P. LOC, *J. Fluid Mech.* **100**, 111 (1980).
17. R. V. MADALA, *Mon. Weather Rev.* **106**, 1735 (1978).
18. S. C. R. DENNIS, in *Proceedings of the Fifth International Conference on Numerical Methods in Fluid Dynamics, 1976*, Lecture Notes in Physics, Vol. 59, edited by A. I. van de Vooren and P. J. Zandbergen (Springer-Verlag, New York/Berlin, 1976), p. 165.